Supporting Online Material

A dynamic knockout reveals that conformational fluctuations influence the chemical step of enzyme catalysis

Gira Bhabha, Jeeyeon Lee, Damian C. Ekiert, Jongsik Gam, Ian A. Wilson, H. Jane Dyson, Stephen J. Benkovic, Peter E. Wright*

*To whom correspondence should be addressed. E-mail: wright@scripps.edu

This PDF file includes:

Supporting Online Material

Materials and Methods

Cloning, expression and purification of mutant DHFR*s*

N23PP/S148A and N23PP E. coli DHFR were generated by site-directed mutagenesis using the QuikChange Multi kit (Agilent) using the wild type template (*1*). The primer sequences are 5'-GAA AAC GCC ATG CCA TGG CCG CCG CTG CCT GCC GAT CTC GCC-3' for the N23PP mutation and insertion, and 5'-GCG CAG AAC GCT CAT AGC TAT-3' for the S148A mutation. Plasmid construction, protein expression, and purification of mutant DHFRs were performed as described previously for kinetic experiments (*1, 2*).

For structural studies, the mutants were over-expressed in BL21(DE3) *E. coli* cells and purified as described previously for wild type *E. coli* DHFR (*3*). The yield of both mutants was ~80 mg/L, significantly greater than the yield of wild type *ec*DHFR. The purified protein was concentrated and used at 800 μM for NMR experiments, and 30 mg/mL for crystallization.

Ligand Preparation

NADPH, $NADP^+$, and folic acid were purchased from Sigma. For kinetic experiments, DHF was synthesized from folate and NADPD [(4'*R*)-^{2}H]NADPH] was synthesized as described in reference (*4*). 6(S)-THF for NMR spectroscopy was purchased from Schircks Laboratories. It should be noted that THF purchased from Sigma (catalog number T3125) may not be suitable for these experiments, as it contains a racemic mixture of 6(S)- and 6(R)-THF, and additionally is only ~65% pure, with the major impurity being folic acid.

Steady-State Kinetics

All kinetic reactions were performed in MTEN buffer (50 mM 2-morpholinoethanesulfonic acid, 25 mM tris(hydroxymethyl)aminomethane, 25 mM ethanolamine and 100 mM NaCl), pH 7.0, containing 5 mM DTT. The k_{cat} values were measured on a Cary 100 BioUV-Vis spectrophotometer (Varian Inc.) at 25 ºC. The enzyme (10-50 nM) was pre-equilibrated with 100 mM NADPH in a 1 mL reaction volume for 3 min, and the reaction was initiated by adding DHF to a final concentration of 100 mM. The change in absorbance was monitored at 340 nm ($D\varepsilon_{340}$ =13.2 mM^{-1} cm^{-1}). For measurements of kinetic isotope effects (KIE), 100 mM NADPD ([(4'*R*)-^{2}H] NADPH) was used instead of NADPH and the ratio of the rates of NADPH/NADPD consumption was calculated to provide the KIE value.

The rate constants associated with the dissociation of the $NADP^+$ and THF from the various product complexes were measured by competitive trapping experiments using a large excess of a second ligand (e.g. methotrexate, NADPH or $NADP^{+)}$. The resultant partial kinetic scheme is shown in Fig. S2.

Pre-Steady State kinetics (Stopped-Flow Measurement)

The pre-steady state reaction rate constants were measured on a stopped-flow instrument (Applied Photophysics Ltd.). For the hydride transfer measurement, fluorescence of NADPH using a 400 nm cutoff filter was monitored. Excitation of the tryptophan residues at 290 nm results in fluorescence emission with a maximum of 340 nm, which is transferred to and excites the NADPH. This leads to an emission maximum of 450 nm. DHFR (5 mM) was preincubated in MTEN buffer with 200 mM of NADPH to avoid hysteresis. Following this, the addition of 200 mM of DHF gave rise to a burst followed by a steady state. Bursts in the pre-steady state were analyzed by a single exponential decay or a single exponential followed by a linear rate.

The pKa values were obtained by measuring a series of burst rates in MTEN buffer at different pHs and pKa values were calculated by fitting the data (shown in Fig. S3B and C) to Equation 1. Data fitting of all kinetic measurements was carried out using Origin or Kaleidagraph software.

$$k_{obs} = k_{min} + (k_{max} - k_{min})/(1+e((pH-pKa)/slope)) \qquad \text{(Equation 1)}$$

As shown in Figure S2, the burst rates are pH-dependent, displaying a decrease in the observed rates with increasing pH. At basic pHs, the hydride transfer rate (k_{hyd}) is decreased to 3.3 s^{-1} (for N23PP/S148A) and 3.2 s^{-1} (N23PP) due to the limited source of protons for the hydride transfer step. The maximal burst rates at pH 5.5, were 31 s^{-1} for N23PP/S148A and 38.5 s^{-1} for N23PP. The pK_a values derived from the pH vs. k_{hyd} profile of the N23PP and N23PP/S148A mutants were 6.6 ± 0.1 and 6.7 ± 0.1, respectively, which are very close to the pK_a of 6.5 for the wild type enzyme (*5*).

Crystallization and Structure Determination

Fractions of N23PP/S148A *ec*DHFR from gel filtration were concentrated to 30 mg/mL and exchanged into buffer containing 10mM Tris, pH 7.5, 1mM DTT using a NAP-5 column, with addition of a 3-fold excess of $NADP^+$ and folic acid. Robotic crystallization trials were carried out using the automated Rigaku Crystalmation platform of the Joint Center for Structural Genomics (JCSG). Only a single crystal was obtained, from a condition consisting of 0.2 M calcium acetate, 0.1 M HEPES, pH 7.5, 40% v/v PEG 400 at 4 °C. The crystal was flash cooled by plunging into liquid nitrogen without any additional cryoprotection. Diffraction data were collected to 1.5 Å resolution at the Advanced Photon Source (APS) General Medicine/Cancer

Institutes Collaborative Access Team (GM/CA-CAT) beamline 23ID-D. Data collection statistics are presented in Table S1.

The dataset was indexed and integrated in $P3_221$ using HKL2000 (HKL Research) and merged using Xprep (Bruker). The structure was solved by molecular replacement using Phaser with 1RX2 as a search model (*6, 7*). A single copy of DHFR was found in the asymmetric unit. Rigid body and restrained refinement were carried out in REFMAC5 (*8*), followed by simulated annealing in Phenix (*9*). Strong, clear electron density was observed for both ligands (Fig. S4). After manual adjustment of the model in Coot (*10*), including rebuilding of the mutated region, ligand placement, and the addition of waters, 2 TLS groups were defined using TLSMD (*11*) and restrained TLS refinement of the structure was completed using REFMAC5. The resulting structure at 1.6 Å resolution was validated using the Quality Control Check v2.7 developed by the Joint Center for Structural Genomics (JCSG) and publically available at http://smb.slac.stanford.edu/jcsg/QC/. Final refinement statistics are presented in Table S1.

NMR spectroscopy

Fractions of ^{15}N labeled N23PP/S148A and N23PP *ec*DHFR from gel filtration were concentrated to 800 μM and exchanged into buffer containing 70 mM potassium phosphate, pH 7.6, 25 mM potassium chloride, 1 mM EDTA, 1 mM DTT, 7% D_2O and 0.02% sodium azide. 10-fold excess of each ligand was added to prepare the desired sample, E:$NADP^+$:FOL or E:$NADP^+$:THF. Because of the insolubility of the folate ligands and, as direct addition of $NADP^+$ drastically lowers the pH, the ligand stock solutions were prepared separately, the pH was adjusted to ~7.5, and the ligands were then added to the protein containing solution. The final pH was adjusted to 7.60 (± 0.03). Since THF is prone to rapid oxidation and degradation when free in solution, all THF samples were prepared in an inert environment, in a glove box

under argon. Backbone assignments were made using standard triple resonance experiments on $^{13}C^{15}N$ labeled protein.

^{15}N R2 relaxation dispersion experiments were measured at 500 MHz and 750 MHz, using constant time CPMG experiments as previously described (*12*). All data were collected at 301 K. The total relaxation period (T_{cpmg}) for all experiments was 40 ms. Data were processed using NMRpipe (*13*) and were fitted as previously described (*3, 14*) using an in-house fitting program, GLOVE. The dispersion curves for residues 127-129, 131, 133, 134, and 157-159 of the N23PP/S148A mutant can be fit with a global k_{ex} value of 590 ± 30 s^{-1}, which is comparable to the rates observed for several complexes of the wild-type enzyme (*15, 16*). It is clear that the dynamics observed in the C-terminal region of DHFR represent a distinct process, unaffected by the Met20 loop mutations and not in any way coupled to the dynamics in the active site. R1, R2 and heteronuclear NOE data were collected at 750 MHz and 301 K. A set of 12 R1 experiments was collected, with relaxation delays of 10, 2000, 80, 1200, 400, 240, 800, 160 and 40 ms, and duplicate points at 10, 400, and 1200 ms. A set of 12 R2 experiments was collected, with relaxation delays of 6, 122, 18, 162, 34, 74, 74, 50, and 98 ms, with duplicate points at 6, 34 and 122 ms. Three sets of data were collected for the heteronuclear NOE experiments, to estimate the error.

Re-refinement of 1RX2

The structure of *E. coli* DHFR bound to $NADP^+$ and folate (PDB code: 1RX2) was released in 1996 and refined using the least squares refinement program TNT (*7*), which was standard at that time. The N23PP/S148A *ec*DHFR structure reported here was refined using REFMAC5, which applies the maximum likelihood (ML) method. ML functions have largely replaced least-squares in macromolecular refinement, as ML consistently produces better models with less bias (*17*). Similarly, as the use of an R_{free} test set was only beginning to be adopted in the mid- to late-1990's, 1RX2 was refined without an R_{free} set. In order to facilitate comparison of the two structures, we wanted to eliminate as many confounding variables as possible between our N23PP/S148A structure and 1RX2. For this reason, we chose to re-refine 1RX2 using the same software and methodologies that we used for N23PP/S148A *ec*DHFR. Because of the absence of an R_{free} set of reflections, it is fair to assume that some bias was introduced into the initial model for 1RX2. For this reason, we used our refined N23PP/S148A *ec*DHFR structure as the initial model, and molecular replaced it into the 1RX2 data before refinement. The differences between using the two initial models is very small, but is noticeable in the region of Met20, as discussed in detail below. The reference wild type *E. coli* DHFR sequence from the NCBI database lists residue 37 as Asn37, while 1RX2 lists the residue as Asp37. This is likely a sequencing error from previous data, and the residue is, in all likelihood, Asn37, even in the 1RX2 structure. However, for consistency with the 1RX2 PDB entry, we have built the residue as Asp37.

Structure factors and coordinates for 1RX2 were obtained from the Protein Data Bank (PDB). The mmcif file containing structure factors was converted to mtz format using the mmcif2mtz tool in the CCP4 suite of programs. Although all reflections had been previously used in refinement, we generated a random R_{free} set comprising ~5% of the reflections. Molecular replacement was carried out with Phaser, using our N23PP/S148A structure as the

initial search model. Several rounds of simulated annealing were performed to attempt to eliminate R_{free} bias from prior refinement against these reflections. All waters and ligands were removed from the coordinates, and the side chain of Met20 was truncated to an alanine prior to refinement. Simulated annealing was carried out in Phenix, followed by restrained TLS refinement (TLS groups generated by TLSMD) using REFMAC5 with manual model building in Coot, essentially as described above for N23PP/S148A *ec*DHFR. The structure was validated using the JCSG's Quality Control Check v2.7.

As discussed briefly in the main text, the re-refined version of 1RX2 is very similar to the original version and also extremely similar to the N23PP/S148A mutant structure. The overall backbone root-mean-square deviation (RMSD) between the wild type and mutant structures is 0.54 Å for all non-hydrogen atoms. Ligand-protein interactions in the active site are maintained (Table S2), and the RMSD for non-hydrogen atoms between active-site residues in the wild-type and mutant structures is 0.25 Å. The positions of waters and the conserved placement of polar side chains in the active site confirm that there is no significant difference between the electrostatic environments of wild-type and N23PP/S148A *ec*DHFRs.

Discussion on Building Met20 and Water 47 into 1RX2-rerefined

The exact rotameric state at the C_γ-S_δ bond of the Met20 sidechain in 1RX2-rerefined is not very clear, but can be modeled as the same rotamer as in N23PP/S148A *ec*DHFR. The Met20 S_δ is shifted ~0.3 Å from its position in the N23PP/S148A *ec*DHFR structure. In addition, we have built in water 47, which was not present in the original structure. Clear electron density is observed for the water, but it is weaker than for the N23PP/S148A structure (Fig. S6). The position is almost identical to the corresponding water in N23PP/S148A, and forms a hydrogen bond to O4 of folic acid. This water has been discussed at length by Sawaya and Kraut (*7*), and is present in other structures of *ec*DHFR. In their insightful discussion a decade ago, it was

especially noted to be present in the open conformation, and thought to be necessary for protonation of the N5 atom of the substrate. Sawaya and Kraut therefore hypothesized that if the open conformation is a structural intermediate between the closed (pre-hydride transfer) and occluded (post hydride transfer) conformations, this water would have intermittent access to the active site, and would be available for protonation of N5. We observe that the water molecule can indeed have access to the active site, even in the closed conformation, in N23PP/S148A *ec*DHFR and in 1RX2-rerefined as well. Neither structure has any crystal contacts in the Met20 loop that could influence the conformation of the loop or the side chains in the loop.

The terminal methyl of Met20 is flexible in the wild-type structure, and probably also in the mutant structure as well. The difference in apparent flexibility between the two structures is likely due to the very different experimental conditions, as data for 1RX2 were collected at 4 °C or at room temperature (*7*), whereas data for N23PP/S148A *ec*DHFR were collected under cryogenic conditions. In solution, the methyl group of the Met20 sidechain in N23PP/S148A is also flexible, and can probably allow intermittent access to the water molecule in the closed conformation. The inherent flexibility of the Met20 methyl group in the E:$NADP^+$:FOL complex has previously been shown for wild-type E:$NADP^+$:FOL using side chain methyl dynamics (*18*). The Met20 methyl group and, by inference, the S_δ atom are quite flexible on the ps-ns timescale. In addition, an analysis of the B-values for the N23PP/S148A *ec*DHFR structure and 1RX2-rerefined indicates that the Met20 sidechain in this crystal is flexible, with higher B-values for the S_δ atom.

1. C. E. Cameron, S. J. Benkovic, *Biochemistry* **36**, 15792 (1997).
2. J. Lee, N. H. Yennawar, J. Gam, S. J. Benkovic, *Biochemistry* **49**, 195 (2010).
3. D. D. Boehr, D. McElheny, H. J. Dyson, P. E. Wright, *Science* **313**, 1638 (2006).
4. S. S. Jeong, J. E. Gready, *Anal Biochem* **221**, 273 (1994).

5. C. A. Fierke, K. A. Johnson, S. J. Benkovic, *Biochemistry.* **26**, 4085 (1987).
6. A. J. McCoy *et al.*, *J Appl Crystallogr* **40**, 658 (2007).
7. M. R. Sawaya, J. Kraut, *Biochemistry.* **36**, 586 (1997).
8. G. N. Murshudov, A. A. Vagin, E. J. Dodson, *Acta Crystallogr. D. Biol. Crystallogr.* **53**, 240 (1997).
9. P. D. Adams *et al.*, *Acta Crystallogr. D. Biol. Crystallogr.* **58**, 1948 (2002).
10. P. Emsley, K. Cowtan, *Acta Crystallogr. D. Biol. Crystallogr.* **60**, 2126 (2004).
11. J. Painter, E. A. Merritt, *Acta Crystallogr. D. Biol. Crystallogr.* **62**, 439 (2006).
12. R. M. Loria J, Palmer III A, *J. Am. Chem. Soc.* **121**, 2331 (1999).
13. F. Delaglio *et al.*, *J. Biomol. NMR* **6**, 277 (1995).
14. D. McElheny, J. R. Schnell, J. C. Lansing, H. J. Dyson, P. E. Wright, *Proc. Natl. Acad. Sci. U. S. A.* **102**, 5032 (2005).
15. D. D. Boehr, H. J. Dyson, P. E. Wright, *Biochemistry.* **47**, 9227 (2008).
16. D. D. Boehr, D. McElheny, H. J. Dyson, P. E. Wright, *Proc. Natl. Acad. Sci. U. S. A.* **107**, 1373 (2010).
17. P. D. Adams, N. S. Pannu, R. J. Read, A. T. Brunger, *Proc. Natl. Acad. Sci. U. S. A.* **94**, 5018 (1997).
18. J. R. Schnell, H. J. Dyson, P. E. Wright, *Biochemistry.* **43**, 374 (2004).

Figure S1. The N23PP/S148A mutant was designed to rigidify the Met20 loop, based on differences between human and *E. coli* DHFRs. **A.** Sequence alignment of wild type *ec*DHFR, N23PP/S148A *ec*DHFR and human DHFR. The site of the N23PP mutation is shown in red, and the site of the S148A mutation in blue. **B.** Structures showing the stabilizing side-chain hydrogen bond in the occluded (left, 1RX4) conformation, which is broken in the closed (right, 1RX2) conformation of *ec*DHFR. The Met20 loop is colored green and folate (yellow), N23 (pink) and S148 (cyan) are rendered as sticks. Secondary structure corresponding to *E. coli* DHFR is shown above the sequence alignment.

A

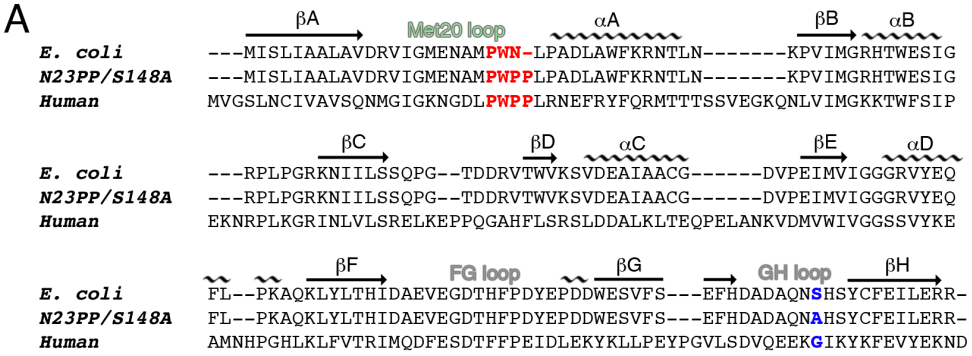

B

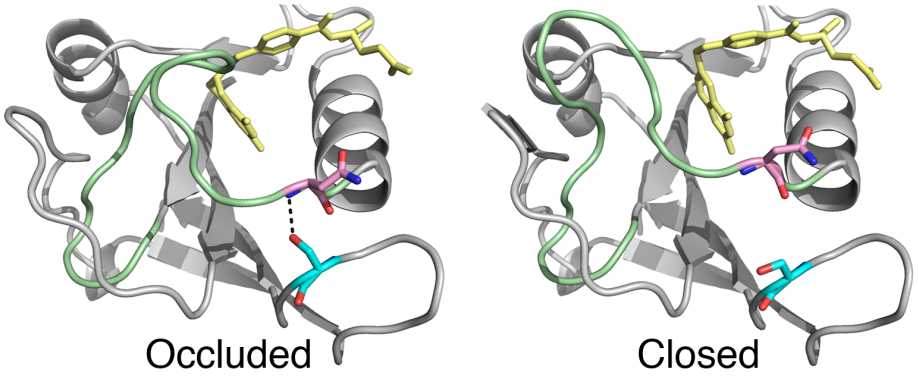

Figure S2
Dissociation rate constants for various product complexes of the N23PP/S148A *ec*DHFR at pH 7.0. The rate constants were measured on a stopped-flow instrument (Applied Photophysics Ltd.). Dissociation of $NADP^+$ from E:$NADP^+$ complex is the rate-limiting step in the catalytic cycle. Note that the rate limiting step of wild type *ec*DHFR reaction is THF dissociation from E:NADPH:THF complex.

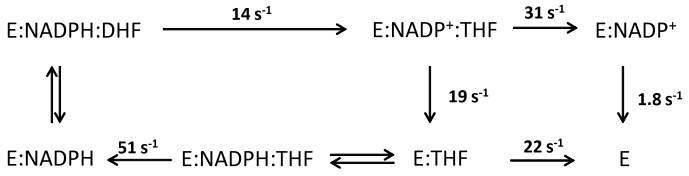

Figure S3
Kinetic data for N23PP/S148A and N23PP *ec*DHFR. **A**. Measurements of a pre-steady state burst rate (k_{hyd}) for the N23PP/S148A mutant DHFR on a stopped-flow instrument. Enzyme (5 mM) was preincubated with a saturating concentration of cofactor (200 mM), and the reaction was initiated by the addition of DHF (200 mM). The solid line represents the fit of the data to a single exponential decay followed by a steady state rate. **B-C**. pH dependence of k_{hyd} for N23PP/S148A DHFR(B) and N23PP(C). The pre-steady state burst rates (k_{hyd}) were measured at different pHs and the pK_as were found to be 6.7 ± 0.1 and 6.6 ± 0.1, respectively.

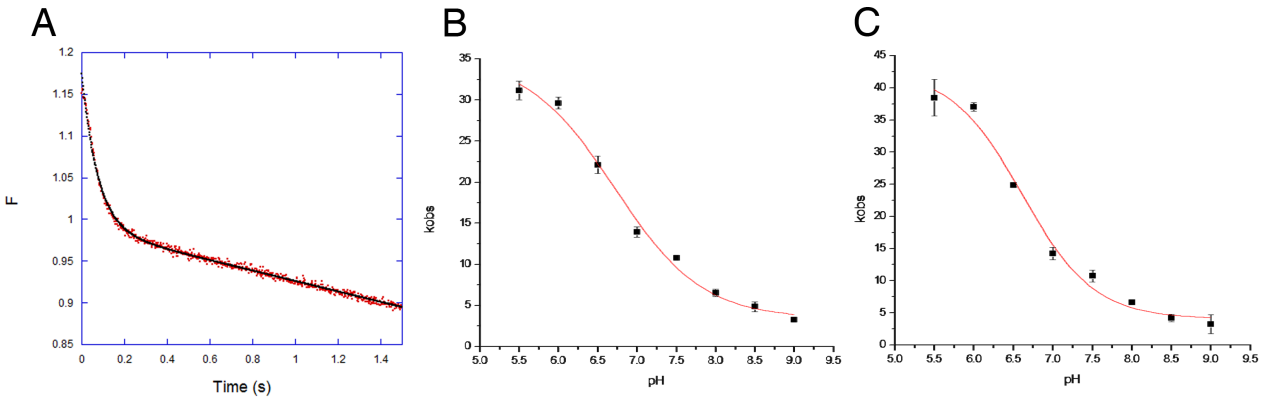

Figure S4
$2F_O$-F_C electron density for folate (**A**) and $NADP^+$ (**B**) ligands in N23PP/S148A ecDHFR structure, contoured at σ=1.0. Unambiguous density was observed for two conformations of the glutamate moiety of folate and both are included in the final models for 1RX2 and N23PP/S148A *ec*DHFR.

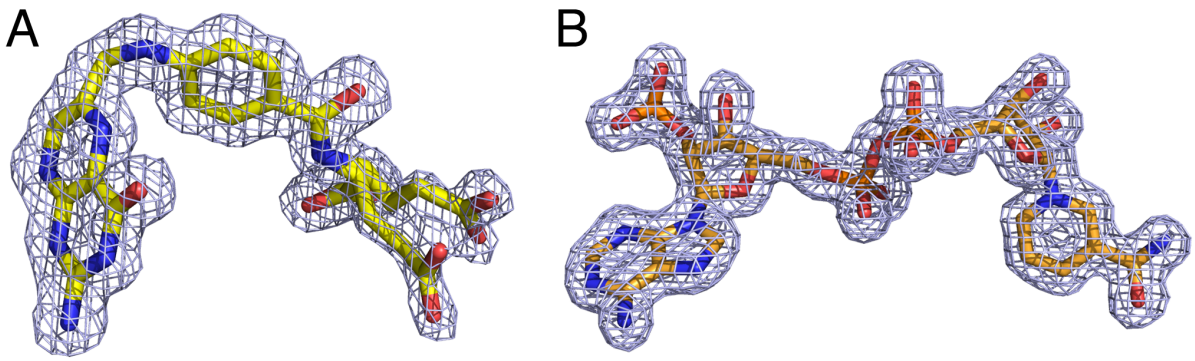

Figure S5
Chemical shift analysis for WT and N23PP/S148A *ec*DHFR. **A.** ^{1}H-^{15}N HSQC spectra for E:NADP^{+}:FOL complexes of wild type (black) and N23PP/S148A (magenta) at 301 K, pH 7.6. **B.** Weighted average ^{1}H, ^{15}N chemical shift differences between wild type and N23PP/S148A E:NADP^{+}:FOL complexes as a function of residue number. The largest chemical shift differences are at the site of the S148A mutation, and reflect the change in residue type rather than a structural change; the difference in the weighted average chemical shift for all other assigned residues is less than 0.3 ppm. Weighted average of chemical shift differences were calculated using the formula:

$$\sqrt{\left(\Delta^{1}H\right)^{2}+\left(\frac{\Delta^{15}N}{5}\right)^{2}}$$

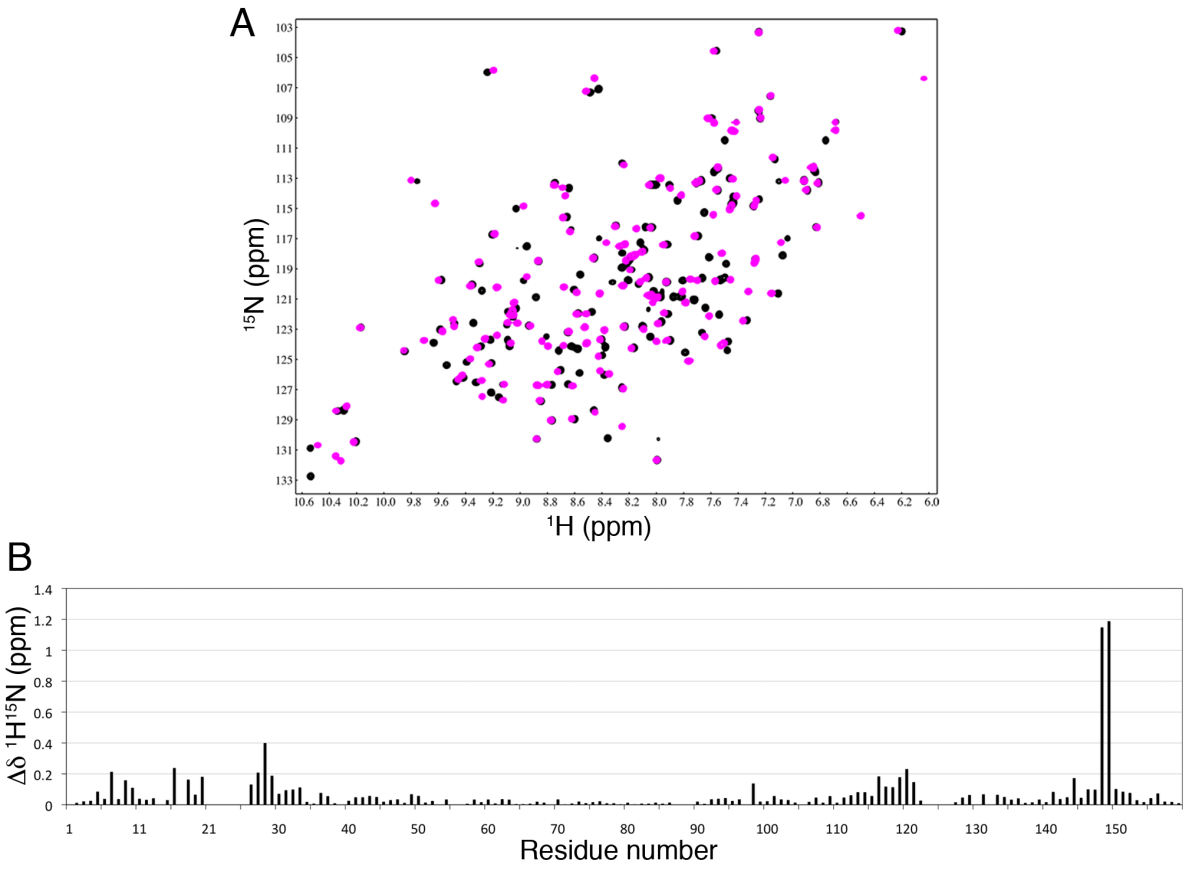

Figure S6
$2F_O$-F_C electron density for Met20 and water 28 in N23PP/S148A ecDHFR (**A, C**) and Met20 and the corresponding water 47 in 1RX2-rerefined (**B, D**). **A.** N23PP/S148A ecDHFR, σ=0.6. **B.** 1RX2-re-refined, σ=0.6. **C.** N23PP/S148A ecDHFR, σ=1.0. **D.** 1RX2-rerefined, σ=1.0. Met20 is shown in green sticks, and the water molecule as a red sphere. Folate is shown in yellow, and $NADP^+$ in orange. The entire Met20 side chain and water 28 are very clearly defined by the electron density in N23PP/S148A ecDHFR. In 1RX2-rerefined, the placement of methyl group of the Met20 side chain and water 47 is more ambiguous. The electron density for the methyl group of Met20 suggests averaging of multiple conformations, and the density for water 47 is weak. The apparent difference in flexibility between the mutant and wild-type Met20 methyl groups is likely due to the difference in the temperatures of the respective data collections: 4 °C or room temperature for 1RX2 and -163 °C for N23PP/S148A ecDHFR.

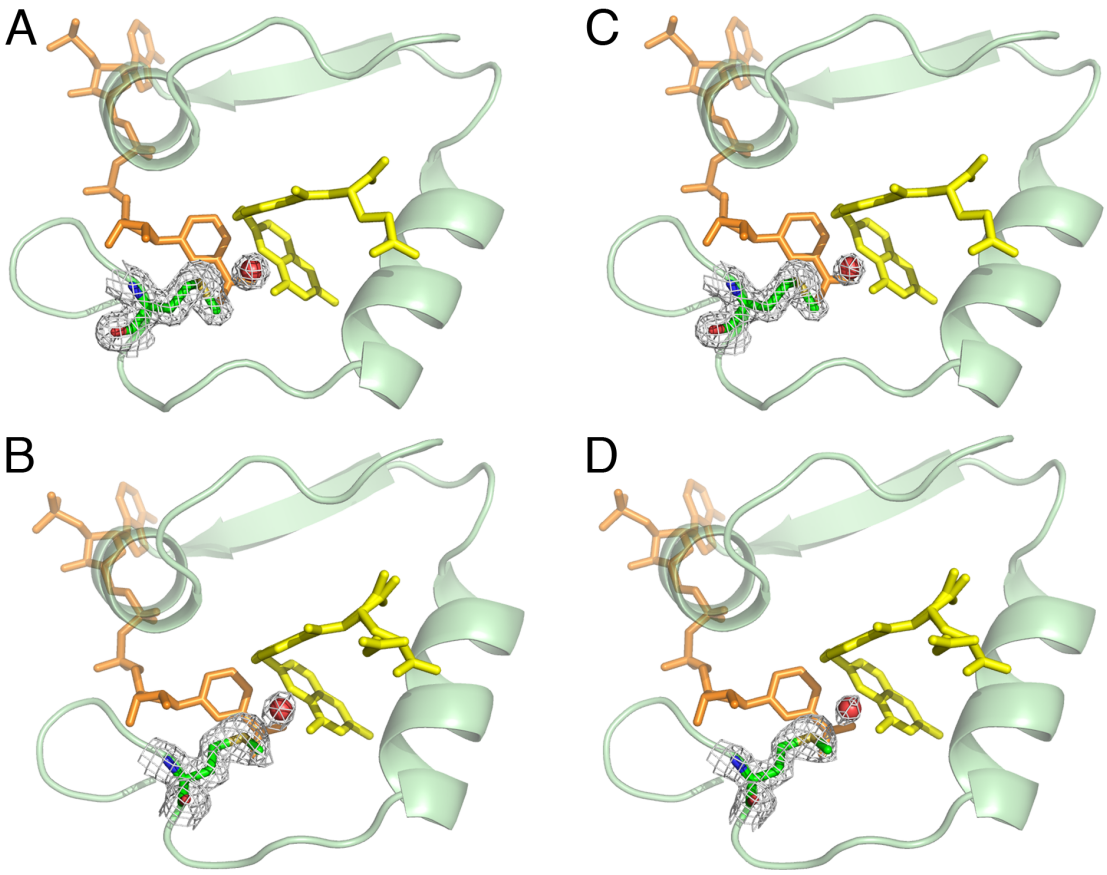

Figure S7
Quantification of the spectra shown in Fig. 3 as a function of residue number. The weighted average ^{1}H, ^{15}N chemical shift differences (calculated as described for Fig. S5) between the E:$NADP^{+}$:FOL and E:$NADP^{+}$:THF complexes are shown in blue for wild type and magenta for N23PP/S148A.

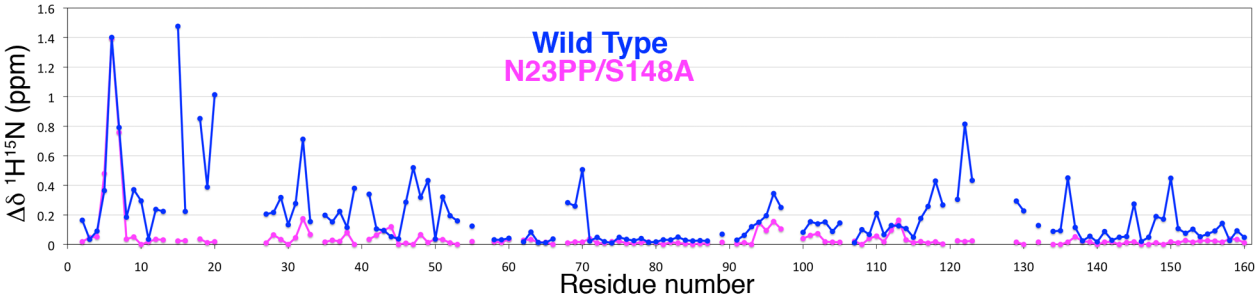

Figure S8
The ps-ns timescale motions are similar for the E:$NADP^+$:FOL complexes of WT and N23PP/S148A *ec*DHFR. ^{15}N R1 (top panel), R2 (middle panel) and heteronuclear NOE values (bottom panel) for wild type (black) and N23PP/S148A (red) *ec*DHFR. The Met20 loop remains fairly rigid on this timescale, as shown by the high average R2 and hnNOE values. Data were collected at 750 MHz and 301 K.

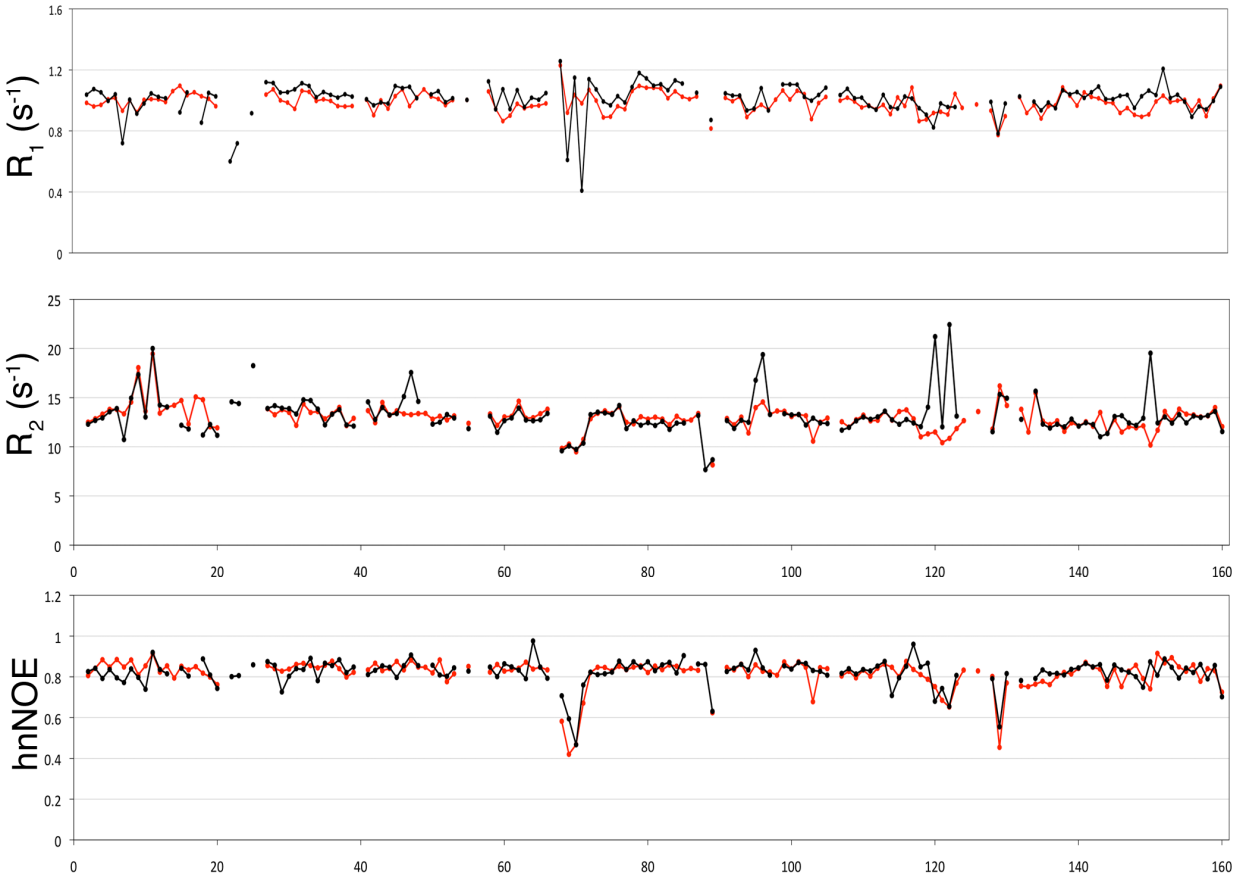

Figure S9
^{1}H-^{15}N HSQC spectra of N23PP *ec*DHFR E:$NADP^{+}$:FOL (black) and E:$NADP^{+}$:THF (red) showing that the N23PP mutation is sufficient to inhibit the closed-to-occluded conformational change across the hydride transfer step. Similar to N23PP/S148A complexes, resonances marking the conformational transition show almost identical chemical shifts in both complexes, and reflect the closed conformation.

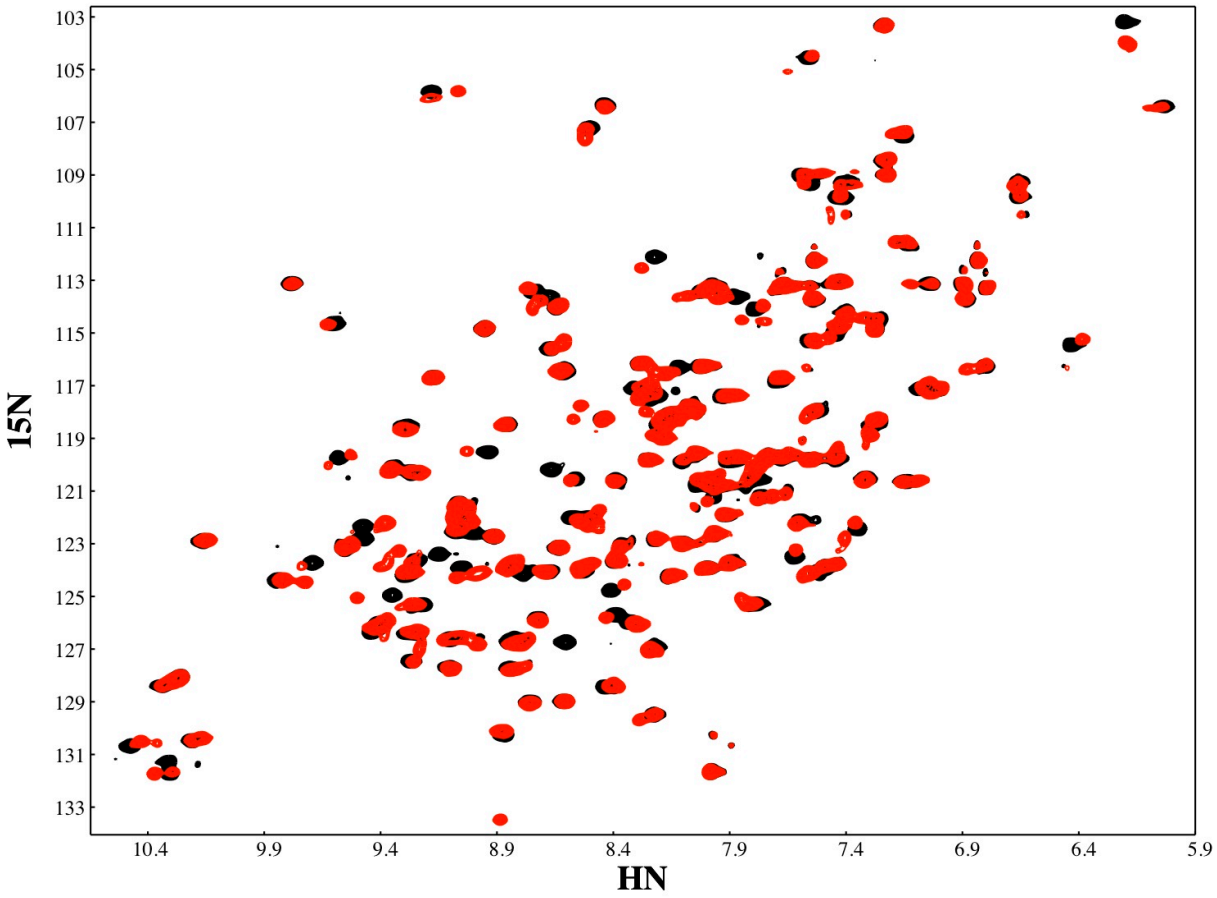

Figure S10
^{1}H-^{15}N HSQC spectra of S148A *ec*DHFR E:$NADP^{+}$:FOL (black) and E:$NADP^{+}$:THF (red) showing that the S148A mutation destabilizes the closed-to-occluded conformational change across the hydride transfer step. Resonances marking the conformational transition show almost identical chemical shifts in both complexes, and reflect the closed conformation.

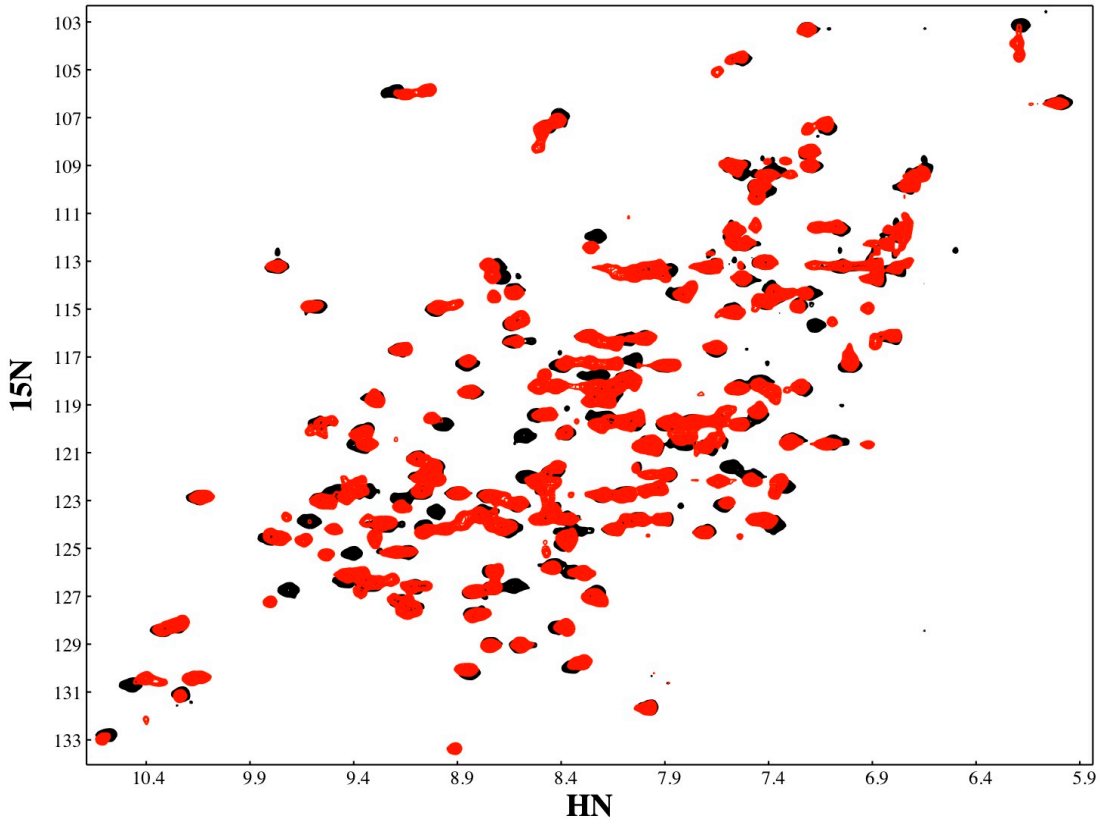

Figure S11
R2 dispersion curves for S148A E:NADP$^+$:FOL active site residues showing dispersion. Red, data collected at 800 MHz; black, data collected at 500 MHz.

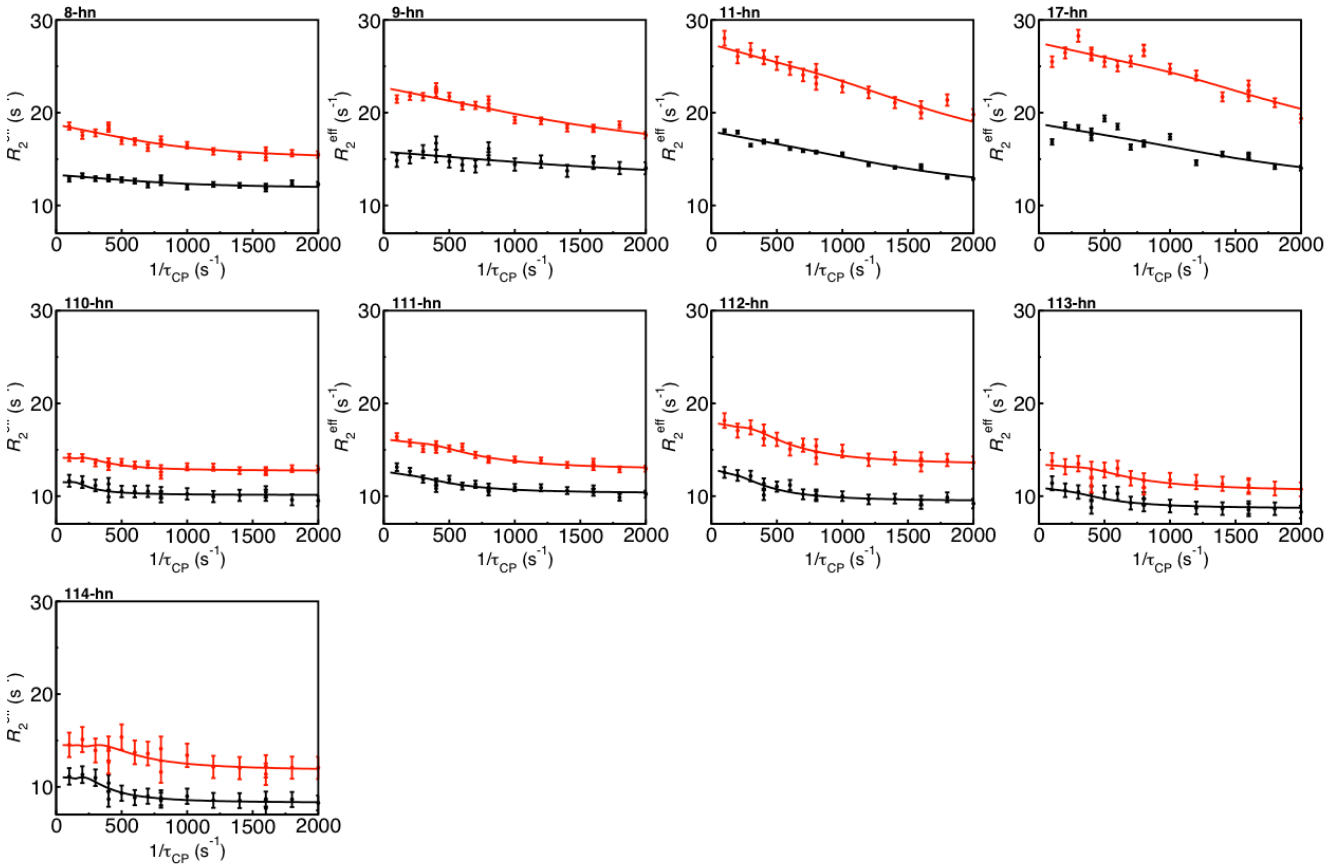

Table S1. Data collection and refinement statistics for crystal structures

Data collection	**N23PP/S148A *ec*DHFR (3QL0)**	**1RX2 Re-refined[f] (3QL3)**
X-ray source	APS GM/CA-CAT 23ID-D	*Rotating anode, Rigaku RU-H2RA*
Wavelength (Å)	1.03333	*1.5418*
Space group	$P3_221$	*$P2_12_12_1$*
Unit cell parameters	a = b = 79.66 Å, c = 71.46 Å $\alpha = \beta = 90.0°, \gamma = 120°$	*a = 34.32 Å, b = 45.51 Å, c = 98.91 Å* *$\alpha = \beta = \gamma = 90.0°$*
Resolution (Å)	50 – 1.59 (1.61 – 1.59)[a]	*100 – 1.8*
Observations	269,590	*64,582*
Unique reflections	35,547 (567)[a]	*14,178*
Completeness (%)	99.6 (97.6)[a]	*94.0*
$\langle I/\sigma_I \rangle$	9.3 (1.8)[a]	*13.5 (2.0)*
R_{sym}[b]	0.08 (0.63)[a]	*0.091*
Refinement statistics		
Resolution (Å)	50-1.60	41-1.8
Reflections (total)	31,133	13,422
Reflections (test)	1639	723
R_{cryst}[c]	20.8	17.7
R_{free}[d]	24.5	21.4
Average B-value (Å^2)		
Protein	17.8	16.2
Ligand 1 ($NADP^+$)	13.6	13.6
Ligand 2 (Folic acid)	17.6	14.2
Water	30.7	22.2
Wilson B-value (Å^2)	13.6	11.4
Protein atoms	1321	1314
Ligand atoms	90	90
Waters	199	75
Other	3	2
RMSD from ideal geometry		
Bond length (Å)	0.011	0.014
Bond angles (°)	1.54	1.54
Ramachandran statistics (%)[e]		
Favored	99.4	100.0
Outliers	0.0	0.0

[a] Numbers in parentheses refer to the highest resolution shell.
[b] $R_{sym} = \Sigma_{hkl} | \langle I_i \rangle | / \Sigma_{hkl} I_i$, where I_i is the scaled intensity of the i^{th} measurement and $\langle I_i \rangle$ is the average intensity for that reflection.
[c] $R_{cryst} = \Sigma_{hkl} | F_o - F_c | / \Sigma_{hkl} | F_o | \times 100$
[d] R_{free} was calculated as for R_{cryst}, but on a test set comprising 5% of the data excluded from refinement.
[e] Calculated using Molprobity.
[f] Data collection statistics are included as reported in the PDB by the authors of 1RX2

Table S2. All hydrogen bonds involving ligands.

N23PP/S148A		Wild type (1RX2)	
Donor	**Acceptor**	**Donor**	**Acceptor**
R57-NH1	FOL-O1	R57-NH1	FOL-O1
R57-NH2	FOL-O2	R57-NH2	FOL-O2
FOL-NA2	D27-OD1	FOL-NA2	D27-OD1
FOL-N3	D27-OD2	FOL-N3	D27-OD2
A7-N	NAP-NO7	A7-N	NAP-NO7
R44-N	NAP-AO4*	R44-N	NAP-AO4*
R44-NE	NAP-AOP2	R44-NE	NAP-AOP2
R44-NH2	NAP-AOP3	R44-NH2	NAP-AOP3
H45-N	NAP-AO5*	H45-N	NAP-AO5*
H45-ND1	NAP-O3	H45-ND1	NAP-O3
T46-N	NAP-AO2	T46-N	NAP-AO2
T46-OG1	NAP-AO2	T46-OG1	NAP-AO2
S63-OG	NAP-AOP2	S63-OG	NAP-AOP2
S64-N	NAP-AOP1	S64-N	NAP-AOP1
S64-OG	NAP-AOP1	S64-OG	NAP-AOP1
G96-N	NAP-AO1		
G96-N	NAP-AO2	G96-N	NAP-AO2
G97-N	NAP-NO5*	G97-N	NAP-NO5*
R98-N	NAP-NO2	R98-N	NAP-NO2
		R98-NH1	NAP-AO3*
		R98-NH2	NAP-AO3*
V99-N	NAP-AO1	V99-N	NAP-AO1
NAP-AN6	Q102-OE1	NAP-AN6	Q102-OE1
NAP-NN7	A7-O	NAP-NN7	A7-O
NAP-NN7	I14-O	NAP-NN7	I14-O
NAP-AN1	K76-O	NAP-AN1	K76-O
		R52-NH2	FOL-O
FOL-N8	NAP-NO7	FOL-N8	NAP-NO7

Table S3. Mean R1, R2 and heteronuclear NOE values for all residues analyzed in wild type and N23PP/S148A *ec*DHFR. Standard deviations are shown in parentheses.

	R1 (s^{-1})	**R2 (s^{-1})**	**hnNOE**	**R2/R1**
Wild type	1.0 (0.1)	13.2 (2.0)	0.82 (0.06)	13.3 (2.8)
N23PP/S148A	0.99 (0.06)	13.0 (1.3)	0.82 (0.07)	13.2 (1.5)